Journal of Solid State Electrochemistry (2019) 23:1089–1097
https://doi.org/10.1007/s10008-019-04200-0

ORIGINAL PAPER

Modeling of oxygen exchange of oxide ceramics: effect of inert particles at the surface

Wolfgang Preis[1]

Received: 17 October 2018 / Revised: 14 January 2019 / Accepted: 16 January 2019 / Published online: 31 January 2019

Abstract

The impact of inert particles located at the surface of mixed ionically/electronically conducting oxide ceramics on the oxygen exchange properties has been studied by numerical modeling of the underlying transport processes. In particular, the phenomenological transport equations have been solved by application of the finite element method. Relaxation curves of the total amount of exchanged oxygen upon an instantaneous change of the oxygen activity in the surrounding atmosphere have been simulated as a function of surface coverage as well as particle size. Both thick samples (thickness, 0.05 cm) and thin samples (thickness, 5 μm) have been investigated. Apparent kinetic parameters, viz. chemical diffusion coefficient and chemical surface exchange coefficient, have been extracted from the simulated relaxation curves by means of nonlinear least squares fitting of appropriate analytical solutions. Basically, the surface exchange reaction is blocked by the inert surface particles, leading to pronounced flux constriction effects. Moreover, in the case of thin samples, relaxation curves can be found which consist of two separate relaxation times. The first time constant is related to the fast relaxation process at free (uncovered) surface regions (usually surface reaction controlled kinetics), while the second relaxation time is caused by two-dimensional diffusion in the thin sample underneath the blocking surface particles.

Keywords Surface exchange reaction · Chemical diffusion · Mixed conducting oxide ceramics · Surface properties

Introduction

The reaction of oxygen in the gas phase with oxide ceramics gives rise to an alteration of the oxygen content (nonstoichiometry) of the mixed ionically/electronically conducting solid phase. Apart from transport processes in the gas phase which are usually negligibly fast, the kinetics of this oxygen exchange process is determined by the surface reaction as well as the diffusion of oxygen in the solid oxide [1–4]. Basically, the transport properties of electroceramic materials are strongly affected by the incorporation of oxygen into the solid oxide during sintering and/or annealing processes. Especially, the electrical properties of interfacially controlled electroceramics, such as $BaTiO_3$-based PTCR (positive temperature coefficient of resistivity) thermistors and ZnO-based varistors, can be tailored by reoxidation during an appropriate thermal treatment [5]. In addition, the polarization resistance of various mixed conducting cathode materials for solid oxide fuel cells (SOFCs) can be correlated with the kinetic parameters, viz. chemical diffusion and surface exchange coefficient, associated with the incorporation of oxygen into the lattice of these materials [6, 7].

Among others, conductivity relaxation experiments are a powerful tool in order to determine the chemical diffusion coefficient $\tilde{D}$ and chemical surface exchange coefficient $\tilde{k}$ of mixed conducting oxide ceramics [8–13]. Moreover, it should be mentioned that a few reports on modeling of conductivity relaxation, including statistical analyses for the determination of $\tilde{k}$ and $\tilde{D}$, can be found in literature (see, e.g., Refs. [3, 14–20]). Furthermore, some recent reports are devoted to long-term measurements of chemical diffusion and surface exchange coefficients in various atmospheres. The reaction of gaseous pollutants with mixed conducting cathode materials might lead to the formation of particles (consisting of, e.g., silicates, sulfates, or carbonates) on the surface, blocking

Electronic supplementary material The online version of this article (https://doi.org/10.1007/s10008-019-04200-0) contains supplementary material, which is available to authorized users.

✉ Wolfgang Preis
wolfgang.preis@unileoben.ac.at

[1] Chair of Physical Chemistry, Montanuniversitaet Leoben, Franz-Josef-Strasse 18, A-8700 Leoben, Austria

the surface exchange reaction owing to their inert behavior [21, 22].

It is the aim of this work to investigate the effect of inert surface particles on relaxation curves of the total amount of exchanged oxygen by application of finite element modeling. Basically, two different models have been developed. The first model contains only one blocking particle on the surface which, however, corresponds to an infinitely large active surface area (cross-section) owing to adequate symmetry boundary conditions. The second model is an array of 25 × 25 surface particles on a surface with an area (cross-section) of 0.5 × 0.5 cm^2. The relation between particle size and surface coverage is identical for both modeling approaches. Mass relaxation curves (time dependence of the total amount of exchanged oxygen), caused by an instantaneous change of the oxygen activity in the ambient atmosphere, have been calculated as a function of surface coverage. Basically, apparent kinetic parameters can be extracted from the simulated relaxation curves which are interpreted in terms of flux constriction effects [23]. Especially, in the case of thin samples (thickness, 5 μm), the overall re-equilibration process shows two different relaxation times. A fast re-equilibration (usually surface reaction controlled) of uncovered active surface regions and a second sluggish relaxation can be distinguished. The second relaxation process can be attributed to slow diffusion underneath the blocking particles.

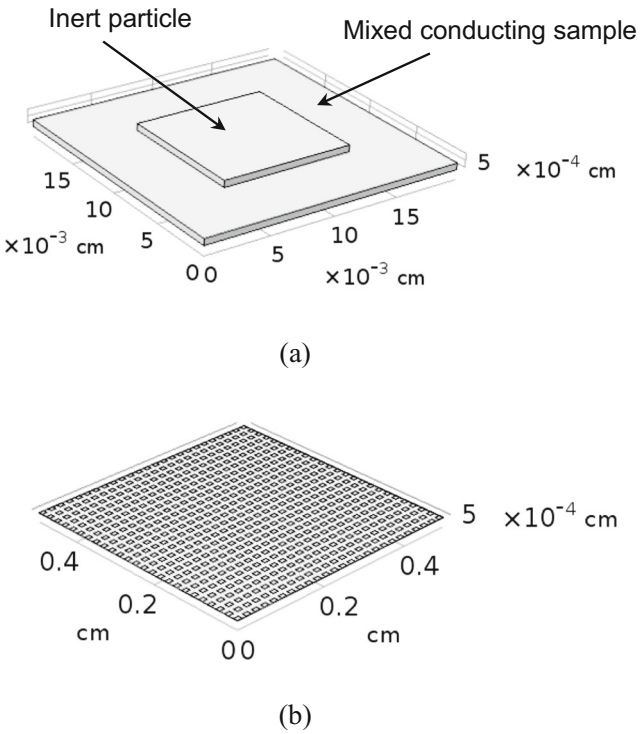

Fig. 1 **a** Model 1: mixed conducting sample with surface area (cross-section) of 0.02 × 0.02 cm^2 and variable thickness (here 5 μm); one inert particle is located at the surface, blocking the surface exchange reaction, with a thickness of 5 μm and variable cross-section (here, 0.01 × 0.01 cm^2 corresponding to a surface coverage of 25%). The faces of the mixed conducting sample perpendicular to the upper (active) surface are blocking for the oxygen exchange reaction (zero flux) corresponding to symmetry boundary conditions, i.e., infinite active surface area. **b** Model 2: mixed conducting sample with surface area (cross-section) of 0.5 × 0.5 cm^2 and a thickness of 5 μm. An array of 25 × 25 inert particles is located at the surface with a thickness of 5 μm and variable size (cross-section) (here, 0.01 × 0.01 cm^2 corresponding to a surface coverage of 25%)

Theoretical considerations

The description of the macroscopic transport process of oxygen through the mixed ionically–electronically conducting ceramic sample is based on the diffusion equation as follows:

$$\frac{\partial c}{\partial t} = \tilde{D}\nabla^2 c \tag{1}$$

with c and $\tilde{D}$ denoting the diffusant concentration (oxygen nonstoichiometry) and chemical diffusion coefficient, respectively. Assuming small deviations from equilibrium (small oxygen partial pressure steps), the boundary condition for the surface exchange reaction can be written as [24, 25]:

$$\tilde{D}\frac{\partial c}{\partial n} = \tilde{k}(c - c_\infty), \tag{2}$$

where $\tilde{k}$ and c_∞ are the chemical surface exchange coefficient and the new equilibrium concentration of the diffusing species (oxygen nonstoichiometry) at the end of the relaxation process, respectively. The operator $\partial/\partial n$ refers to differentiation along the normal of the surface. The basic geometry of a sample with inert particles on its surface is sketched in Fig. 1. Oxygen exchange is assumed to occur exclusively at the upper surface covered by inert particles. The remaining surfaces of the specimen may be blocking for the oxygen exchange reaction, i.e., vanishing fluxes:

$$\frac{\partial c}{\partial n} = 0 \tag{3}$$

Due to the inert nature of the surface particles, the boundary condition (3) is fulfilled at all surfaces of the inert particle (the chemical diffusion coefficient and surface exchange coefficient of the particles are extremely small: $\tilde{D}_p \to 0, \tilde{k}_p \to 0$). In addition, the interface between the inert particle and the specimen may likewise be blocking for the oxygen transport:

$$\tilde{D}\frac{\partial c}{\partial n} = \tilde{D}_p \frac{\partial c_p}{\partial n} = k'\left(c' - c_p'\right) = 0 \tag{4}$$

with $\tilde{D}_p$, c_p, $k' \to 0$, c', and c_p' corresponding to the chemical diffusivity as well as concentration of the diffusing species of the inert particle, the mass transfer coefficient for transport across the interface, and the diffusant concentrations of the

blocking boundary layer (negligibly small thickness) in contact with the sample and inert particle, respectively.

The effect of inert surface particles on the oxygen exchange process is investigated by means of finite element models in order to solve numerically the diffusion Eq. (1) with boundary conditions (2)–(4). The finite element simulations were performed by application of COMSOL Multiphysics 5.3a©. Figure 1a shows model 1 where one inert particle is located on the surface. As the sample surfaces perpendicular to the active surface are diffusion barriers (symmetry boundary conditions), this geometry resembles a sample with an infinite large surface area (cross-section). Usually, the thickness of the surface particles is confined to 5 μm (except for the case of a particle size of 1 μm where cubic particles were used). The surface coverage was altered for a constant particle size (constant side length) by variation of the sample side length. In the case of variable particle size, the particle side length was varied, while the sample side length was maintained constant (e.g., 0.02 cm). Both thin and thick sample geometries were studied by variation of the sample thickness, i.e., $L = 5$ μm and 0.05 cm, respectively. Furthermore, Fig. 1b shows model 2 comprising a thin sample (thickness, 5 μm) with a side length of 0.5 cm (cross-section, 0.25 cm^2) covered by an array of 25×25 identical particles. Again, the particle thickness was confined to 5 μm (with cubic particles in the case of a particle size of 1 μm), and the surface coverage was varied by a systematic variation of the particle side length. The relationship between side length of the inert surface particles and the surface coverage for both models is depicted in Fig. 2. It is worth mentioning that typically the mesh for model 1 consists of more than 10^5 tetrahedral elements, while model 2 is composed of more than 10^6 tetrahedral elements (further details can be found in the supplementary material). In both cases, a parallel sparse direct solver (MUMPS implemented in COMSOL Multiphysics©) has been utilized for solving the diffusion equations.

The total amount of exchanged oxygen can be obtained from the volume integral of the normalized diffusant concentration (oxygen nonstoichiometry):

$$\frac{m(t)}{m(\infty)} = \frac{1}{V}\int_V c_{\mathrm{norm}}\mathrm{dV}; c_{\mathrm{norm}} = \frac{c - c_0}{c_\infty - c_0} \tag{5}$$

with c_0 and c_∞ denoting the initial and final diffusant concentrations for $t = 0$ and $t \to \infty$, respectively, and V corresponds to the sample volume.

Results and discussion

A typical result for the finite element simulation of the oxygen exchange process employing model 1 for a sample with a thickness of 0.05 cm and a surface coverage of 75% (side length of inert particle: 0.01732 cm; side length of the upper (active) surface of the sample, 0.02 cm) is illustrated in Fig. 3. The slice plot for the normalized diffusant concentration in Fig. 3 clearly indicates the hindrance of the oxygen exchange at the surface by the inert particle. The transport process is no longer one-dimensional owing to flux constriction effects [23] caused by the blocking surface particle. Nonetheless, apparent $\tilde{k}$ and $\tilde{D}$ values can be extracted from the simulated relaxation curves (based on Eq. (5)) by nonlinear least squares fitting of the one-dimensional analytical solution [25–28]. If the transport process was one-dimensional, a linear relation between the apparent surface exchange coefficient and the surface coverage of inert particles would be expected, viz. $\tilde{k} = \tilde{k}_{\mathrm{input}}(1-g)$, g denotes the surface coverage. However, flux constriction effects give rise to a nontrivial relationship between the apparent kinetic parameters ($\tilde{k}$ and $\tilde{D}$) and the surface coverage, as can be seen in Fig. 4. The dashed line in Fig. 4a corresponds to the linear correlation between the surface exchange coefficient and the surface coverage of blocking particles. The results of the finite element simulations for the free sample surface (zero coverage) deviate somewhat from the input parameter $\tilde{k}_{\mathrm{input}} = 5 \times 10^{-4}$ cm s^{-1} because of small numerical inaccuracies (the numerical uncertainty is around 7%). However, in the case of surface reaction controlled kinetics, i.e., $\tilde{k}L/\tilde{D} < 0.3$, a linear relationship between the apparent surface exchange coefficient, extracted from simulated relaxation curves, and the surface coverage can be observed. Figure 4a reveals that in the case of diffusion controlled or mixed surface reaction/diffusion-controlled kinetics of the oxygen exchange process significant deviations between the linear relationship (dashed line) and the simulated results can be found. The deviations increase with decreasing $\tilde{D}_{\mathrm{input}}$ values owing to enhanced flux constriction effects. On

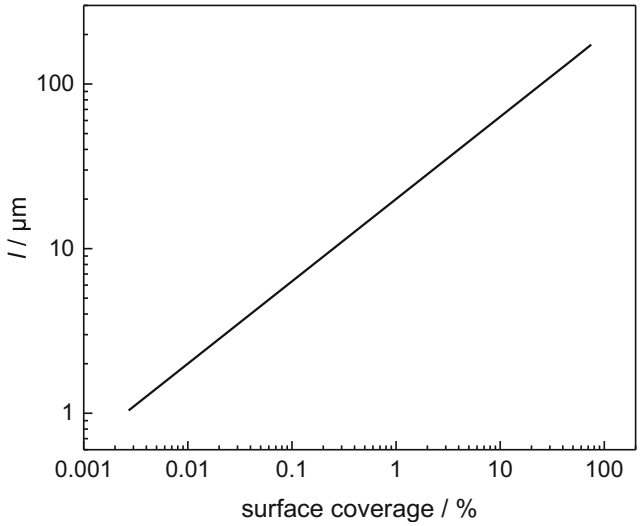

Fig. 2 Variation of side length (size) of inert surface particles with surface coverage for both finite element models

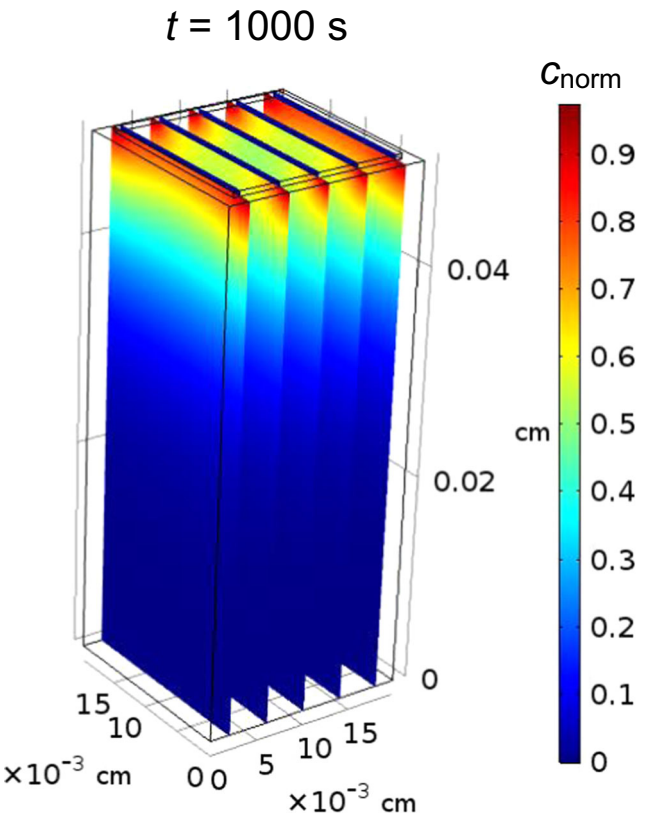

Fig. 3 Slice plot of normalized diffusant concentration after a relaxation time of 1000 s using model 1. Sample thickness, 0.05 cm; cross-section, 0.02×0.02 cm^2; particle size, 0.017321 cm (surface coverage, 75%); $\tilde{k}_{\text{input}} = 5 \times 10^{-4}$ cm s^{-1}; $\tilde{D}_{\text{input}} = 10^{-7}$ cm^2 s^{-1}

the contrary, the apparent diffusion coefficients are independent of the surface coverage and agree closely with the pertinent input parameters, as can be seen in Fig. 4b. It should be noted that similar results have been reported in Ref. [23], where flux constriction effects have been modeled with respect to active surface sites, such as catalytically active porous Pt electrodes on mixed conducting or ionically conducting oxide ceramics.

In addition, the effect of blocking surface particles on the oxygen exchange kinetics of a thin sample with a thickness of 5 μm has been investigated by application of both model 1 and model 2. A typical simulation result using model 2 is depicted in Fig. 5. Although the oxygen exchange kinetics is surface reaction controlled (thin sample), the transport process is no longer one-dimensional. Basically, the regions at the free (uncovered) surface show fast (surface reaction controlled) equilibration, whereas slow lateral transport occurs underneath the blocking surface particles especially in the case of fairly small diffusion coefficients (see, Fig. 5). These transport processes may give rise to relaxation curves with two different relaxation times. From Fig. 6a, one can deduce that relaxation curves for the total amount of exchanged oxygen, consisting of two separate time constants, can be found for surface coverages of 25 and 75%, respectively. The fairly fast equilibration of a thin sample with only 0.068% coverage of blocking particles shows one relaxation time. The two different relaxation times are even better visible in the semilogarithmic plots provided in Fig. 6b, where the slope of linear regions corresponds to the pertinent relaxation time, τ, viz. $\mathrm{d}\ \ln[1 - m(t)/m(\infty)]/\mathrm{d}\ t = -1/\tau$. Basically, the first relaxation can be related to the fast re-equilibration of the free surface regions:

$$\tau_1 \approx \frac{L}{\tilde{k}_{\text{input}}} \tag{6}$$

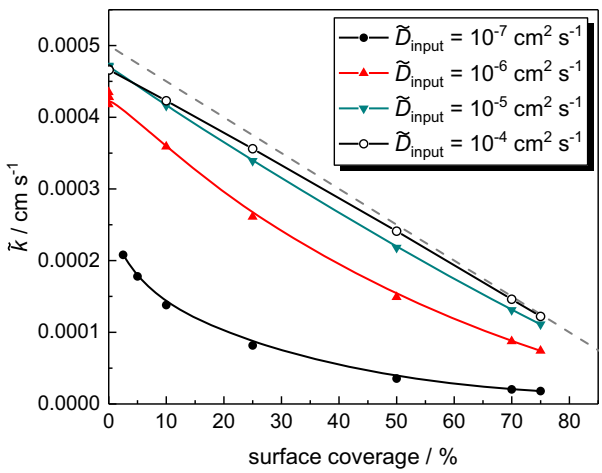

(a)

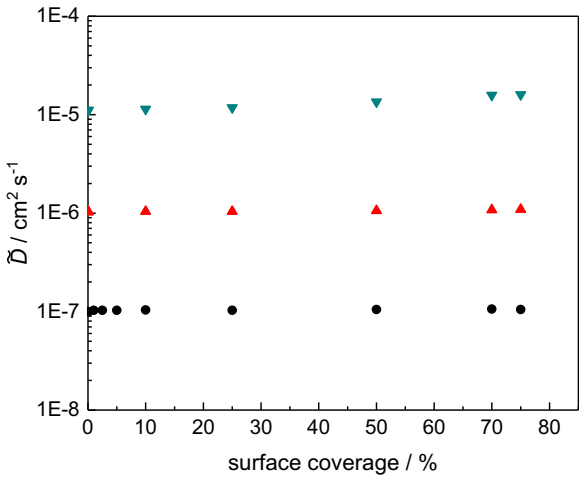

(b)

Fig. 4 **a** Variation of apparent chemical surface exchange coefficient, extracted from simulated relaxation curves by fitting the one-dimensional analytical solution, with surface coverage. **b** Variation of apparent chemical diffusion coefficient, extracted from simulated relaxation curves by fitting the one-dimensional analytical solution, with surface coverage. Finite element simulations are based on model 1: sample thickness, 0.05 cm; cross-section, 0.02×0.02 cm^2; $\tilde{k}_{\text{input}} = 5 \times 10^{-4}$ cm s^{-1}

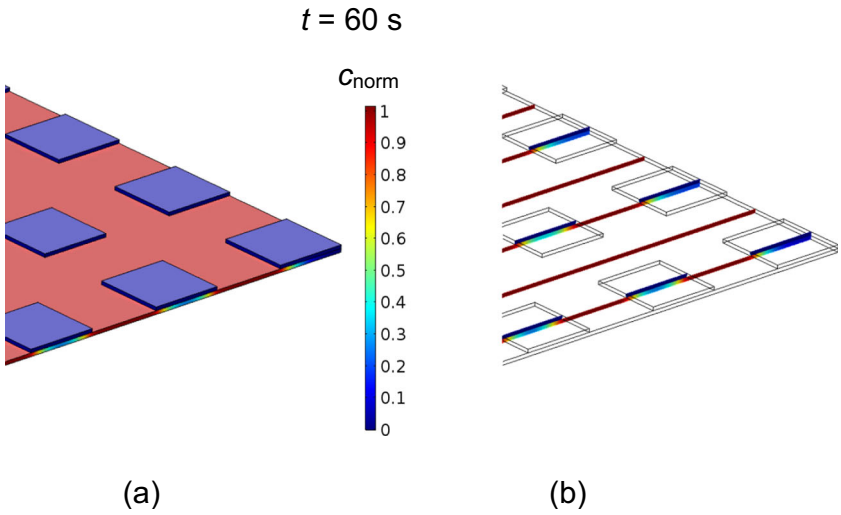

Fig. 5 Finite element simulation using model 2: magnified detail of normalized diffusant concentration after a relaxation time of 60 s. Sample thickness, 5 μm; cross-section, 0.5 × 0.5 cm^2; particle size, 0.01 cm (surface coverage, 25%); $\tilde{k}_{input} = 5 \times 10^{-4}$ cm s^{-1}; $\tilde{D}_{input} = 10^{-7}$ cm^2 s^{-1}. **a** Surface plot; **b** slice plot

where L refers to the sample thickness. The second relaxation time is caused by the lateral two-dimensional diffusion process underneath the surface particles:

$$\tau_2 \approx \frac{l^2}{2\tilde{D}_{input}\pi^2} \tag{7}$$

with l being the length of the surface particle (the correlation between particle length and surface coverage for both model 1 and 2 is plotted in Fig. 2). Obviously, these two relaxation processes can only be observed, if the difference between the time constants is large enough, i.e., $\tau_1 \ll \tau_2$. Hence, a condition for the occurrence of two separate relaxation processes in the case of thin samples covered by blocking surface particles can be derived as follows:

$$l^2 \gg \frac{2\tilde{D}_{input}\pi^2}{\tilde{k}_{input}} L \tag{8}$$

or more roughly: $l^2 \gg \tilde{D}_{input} L / \tilde{k}_{input}$. In the case of somewhat higher diffusivities or a small particle size (small l), the two different relaxation processes will still occur. However, a clear separation is not possible because relation (8) is no longer fulfilled. Examples for relaxation curves consisting of only one relaxation time are shown in Fig. 7. In this case, apparent kinetic parameters can be obtained by fitting the one-dimensional analytical solution [25–28] to the simulated relaxation curves. A more detailed description of re-equilibration involving two separate relaxation processes can be found in the Appendix.

The variation of the apparent surface exchange coefficient with surface coverage is depicted in Fig. 8a, and the apparent diffusion coefficient is plotted as a function of surface coverage in Fig. 8b. The gray solid line in Fig. 8a (logarithmic x-axis for better visibility of small coverages) indicates the linear relationship between $\tilde{k}$ and the surface coverage, $\tilde{k} = \tilde{k}_{input}(1-g)$, with g referring to the surface coverage. In the case of a fairly small particle size ($l = 1$ μm), the finite element simulations show only one relaxation time and the extracted $\tilde{k}$ values are in close agreement with the linear relationship (see, Fig. 8a). Moreover, the apparent $\tilde{D}$ values are independent of the surface coverage and concur well with the corresponding input parameter. In the case of larger particles ($l = 5$ μm), exclusively small (almost negligible) surface coverage resulted in relaxation curves with only one relaxation time. Furthermore, the particle size has been varied

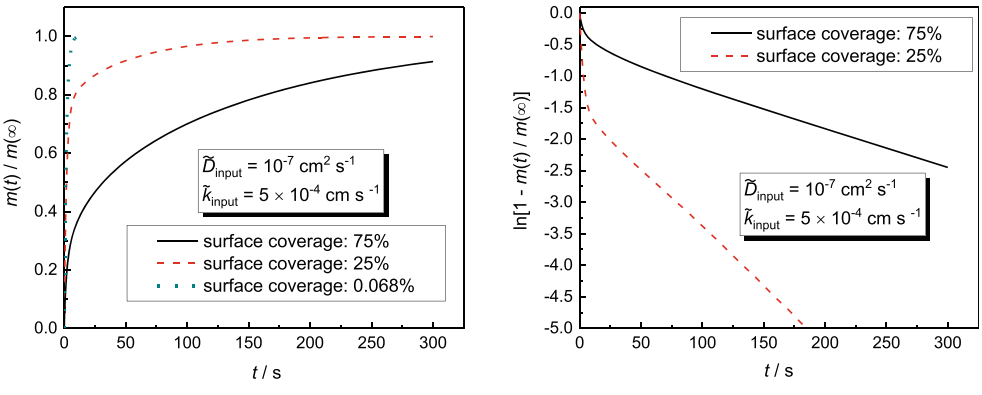

Fig. 6 Relaxation curves for the total amount of exchanged oxygen as a function of surface coverage. **b** Semilogarithmic plot of $\ln[1 - m(t)/m(\infty)]$ versus time for various surface coverages. The finite element simulations are based on model 1: sample thickness, 5 μm; cross-section, 0.02 × 0.02 cm^2; $\tilde{k}_{input} = 5 \times 10^{-4}$ cm s^{-1}; $\tilde{D}_{input} = 10^{-7}$ cm^2 s^{-1}

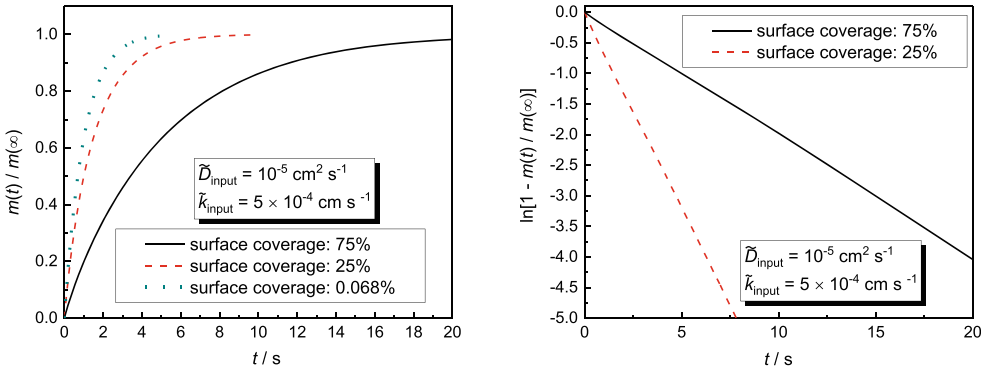

(a) (b)

Fig. 7 **a** Relaxation curves for the total amount of exchanged oxygen as a function of surface coverage. **b** Semilogarithmic plot of $\ln[1 - m(t)/m(\infty)]$ versus time for various surface coverages. The finite element simulations are based on model 1: sample thickness, 5 μm; cross-section, 0.02×0.02 cm^2; $\tilde{k}_{input} = 5 \times 10^{-4}$ cm s^{-1}; $\tilde{D}_{input} = 10^{-5}$ cm^2 s^{-1}

systematically (the relation between particle size and surface coverage can be seen in Fig. 2 for model 1 as well as model 2). The relaxation curves (see, Fig. 7) are composed of one relaxation time, such that apparent kinetic parameters could be obtained. According to Fig. 8a, the apparent $\tilde{k}$ values deviate significantly from the linear relationship. Interestingly, the apparent surface exchange coefficients are too high. Figure 8b reveals that the apparent $\tilde{D}$ values are lower than the pertinent input parameter by almost two orders of magnitude. Thus, the relaxation process seems to be mixed controlled instead of k controlled as expected from the input parameters. Relaxation curves for a surface coverage of 75% using model 1 (particle size $l = 173.2$ μm) are shown in Fig. 9a for various input parameters of the chemical diffusion coefficient. Two different transport processes can clearly be observed with regard to $\tilde{D}_{input} = 10^{-7}$ cm^2 s^{-1}. When the chemical diffusivity is increased, the two separate relaxation times will merge into one effective time constant. However, the interpretation of this effective relaxation process is only meaningful, if the condition $\tau_{eff} \gg \tau_2$ is valid with $\tau_{eff} = L/\left[\tilde{k}_{input}(1-g)\right]$ and $\tau_2 = l^2/\left(2\tilde{D}_{input}\pi^2\right)$. Hence, the condition for a linear behavior of the apparent surface exchange coefficient as a function of the surface coverage reads as follows:

$$l^2 \ll \frac{2\tilde{D}_{input}\pi^2}{\tilde{k}_{input}(1-g)}L \tag{9}$$

which can be simplified to $l^2 \ll \tilde{D}_{input}L/\left[\tilde{k}_{input}(1-g)\right]$. Condition (9) is certainly valid with regard to $\tilde{D}_{input} = 10^{-4}$ cm^2 s^{-1} in Fig. 9. Thus, the apparent k values extracted from the simulated relaxation curves decrease linearly with decreasing surface coverage, as can be seen in Fig. 10. It should be noted that in the case of D-controlled kinetics, two distinct time regimes can be observed. The short-time regime is characterized by $m(t)/m(\infty) \propto \sqrt{t}$ (square-root behavior of the diffusion process), while the long-time regime is consistent with $\ln[1-m(t)/m(\infty)] \propto -\tilde{D}\pi^2 t/L^2$, where the intercept at the y-axis of the semilogarithmic plot $\ln[1 - m(t)/m(\infty)]$ versus time is given by $\ln(8/\pi^2) = -0.21$. In the case of k-controlled kinetics, the

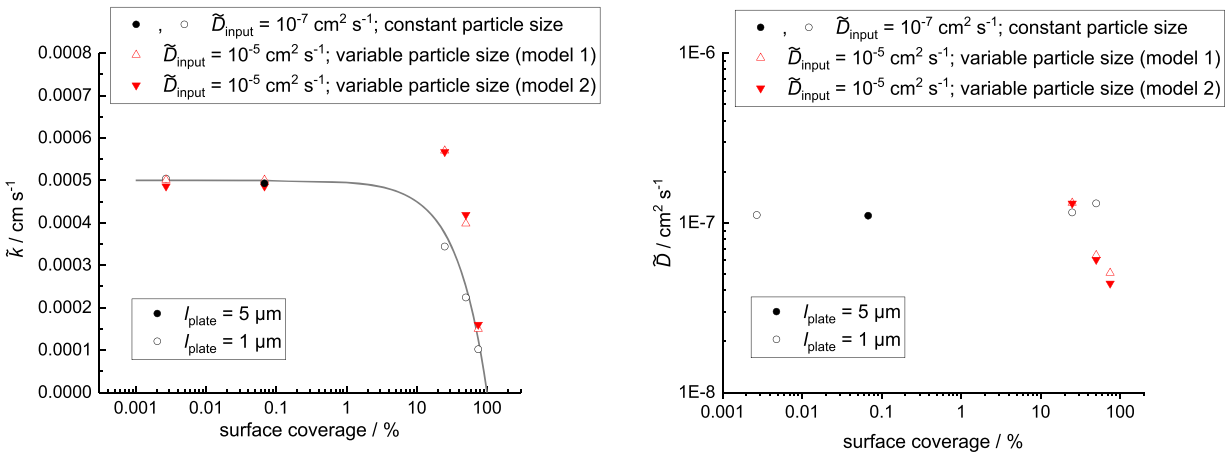

(a) (b)

Fig. 8 **a** Apparent chemical surface exchange coefficient plotted as a function of surface coverage. **b** Apparent chemical diffusion coefficient plotted as a function of surface coverage. The apparent kinetic parameters are obtained from fitting the one-dimensional analytical solution to the simulated relaxation curves based on both model 1 and 2. The surface coverage has been varied for constant particle size (model 1) as well as variable particle size (models 1 and 2); $\tilde{k}_{input} = 5 \times 10^{-4}$ cm s^{-1}

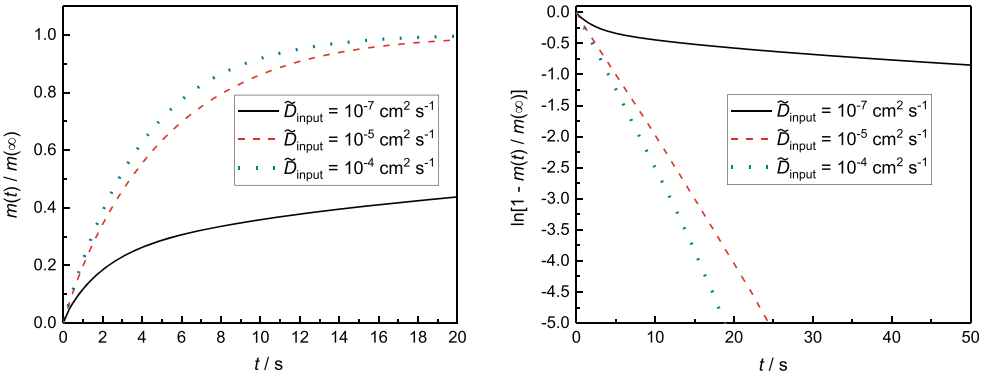

(a) (b)

Fig. 9 **a** Relaxation curves for the total amount of exchanged oxygen for various input parameters of the chemical diffusion coefficient (surface coverage, 75%, model 1). **b** Semilogarithmic plot of $\ln[1 - m(t)/m(\infty)]$ versus time for various input parameters of the chemical diffusion coefficient (surface coverage, 75%, model 1). Sample thickness, 5 μm; cross-section, 0.02×0.02 cm^2; $\tilde{k}_{\text{input}} = 5 \times 10^{-4}$ cm s^{-1}

semilogarithmic plot $\ln[1 - m(t)/m(\infty)]$ versus time shows a linear behavior with $\ln[1-m(t)/m(\infty)] \propto -\tilde{k}t/L$ and the intercept at the y-axis is zero, i.e., short- and long-time regimes can no longer be distinguished. The situation for mixed k- and D-controlled kinetics is in between. A more detailed discussion can be found elsewhere [26, 27]. The increase of $\tilde{D}_{\text{input}}$ leads to gradual vanishing of the intercept at the y-axis (see, Fig. 9b), such that the simulated relaxation curves would erroneously reflect mixed controlled oxygen exchange kinetics although the overall transport process is composed of two different relaxation processes which cannot be deconvoluted properly. The input parameter $\tilde{D}_{\text{input}} = 10^{-5}$ cm^2 s^{-1} refers to the latter situation, yielding wrong apparent $\tilde{k}$ and $\tilde{D}$ values illustrated in Figs. 8 and 10.

Finally, it is worthwhile mentioning that in accordance with Fig. 8, the simulation results obtained from models 1 and 2 are in close agreement. Additionally, it should be noted that both models 1 and 2 are characterized by an identical relationship between surface particle size and surface coverage shown in Fig. 2. As model 1 corresponds to a sample with an infinite active surface area (because of the symmetry boundary conditions), it can be concluded that even an array of 25×25 inert particles on a surface with an area (cross-section) of 0.5×0.5 cm^2 is sufficient for a proper calculation of the oxygen exchange process applying finite element models. Moreover, it should be mentioned that model 2 would provide the basis for further studies concerning the effect of different distributions of particle size and shape on the oxygen exchange kinetics.

Summary

The effect of inert surface particles on the oxygen exchange kinetics of mixed ionically/electronically conducting oxide ceramics has been investigated by application of finite element modeling. Two types of finite element models have been created. The first model consists of one surface particle on a surface of 0.02×0.02 cm^2 and is based on symmetry boundary conditions, such that the area (cross-section) of the active surface is infinitely large. The second model comprises an array of 25×25 particles on a surface with a cross-section of 0.5×0.5 cm^2. It should be mentioned that the variation of the

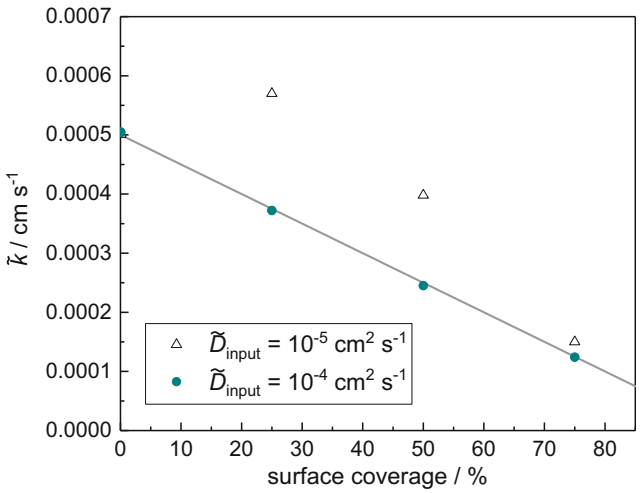

Fig. 10 Plot of apparent chemical surface exchange coefficient versus surface coverage for various input parameters of the chemical diffusion coefficient using model 1. Sample thickness, 5 μm; cross-section, 0.02×0.02 cm^2; $\tilde{k}_{\text{input}} = 5 \times 10^{-4}$ cm s^{-1}

particle size with surface coverage is virtually identical for both models. Basically, the simulation results are in close agreement for both models. Moreover, the effect of inert surface particles on the transport processes have been studied on a thick sample (thickness, 0.05 cm) as well as a thin specimen (thickness, 5 μm). In the former case, a linear relationship between apparent surface exchange coefficients, extracted from simulated relaxation curves by fitting the analytical solution for one-dimensional transport, and the surface coverage has been found exclusively with regard to *k*-controlled kinetics for the oxygen exchange process. If, in turn, the oxygen exchange process is *D*-controlled or mixed *k*- and *D*-controlled, the decrease of the apparent surface exchange coefficient with increasing surface coverage of blocking particles is no longer linear which can be attributed to nontrivial flux constriction effects. In the case of a thin sample, the situation is even more complicated, as two different transport processes may occur. A fast relaxation process is caused by usually *k*-controlled re-equilibration of free (uncovered) surface regions, whereas the additional lateral (two-dimensional) diffusion underneath the blocking surface particles gives rise to a second (sluggish) relaxation process. This peculiar behavior will vanish and relaxation curves with only one effective time constant will be found, if the diffusivity is large and/or the particle size as well as surface coverage are small. In this case, the apparent (effective) surface exchange coefficients associated with the effective relaxation times show a linear dependence on the surface coverage as expected for one-dimensional *k*-controlled relaxation kinetics.

Appendix

The oxygen exchange of thin samples can be described by the analytical approximation for the total amount of exchanged oxygen involving two separate relaxation processes:

$$\frac{m(t)}{m(\infty)} = 1-g\left(\frac{8}{\pi^2}\right)^2 \sum_{m=1}^{\infty}\sum_{n=1}^{\infty} \frac{\exp\left[-\tilde{D}(2m-1)^2\pi^2 t/l_1^2\right]}{(2m-1)^2} \times \frac{\exp\left[-\tilde{D}(2n-1)^2\pi^2 t/l_2^2\right]}{(2n-1)^2} - \\ -2(1-g)\left(\frac{\tilde{k}}{\tilde{D}}\right)^2 \sum_{i=1}^{\infty} \frac{\exp\left(-\alpha_i^2\tilde{D}t\right)}{\alpha_i^2\left(\tilde{k}^2L^2/\tilde{D}^2 + \tilde{k}L/\tilde{D} + L^2\alpha_i^2\right)} \tag{A1}$$

where the parameters α_i are the roots of the transcendental equation:

$$\alpha_i \tan(\alpha_i L) = \frac{\tilde{k}}{\tilde{D}} \tag{A2}$$

and g denotes the surface coverage. In the case of square-shaped surface particles, as employed in the present finite element model, l_1 equals l_2, i.e. $l_1 = l_2 = l$. The two separate time constants can be written as follows:

$$\tau_1 = \frac{1}{\alpha_1^2\tilde{D}} \tag{A3}$$

and

$$\tau_2 = \frac{l_1^2 l_2^2}{\left(l_1^2 + l_2^2\right)\tilde{D}\pi^2} \tag{A4}$$

which are consistent with Eqs. (6) and (7) in the case of *k*-controlled kinetics at the free (uncovered) surface regions and $l_1 = l_2 = l$ (square-shaped surface particles). It is important to note that Eq. (A1) is only valid, if $\tau_1 \ll \tau_2$ is fulfilled. Figure 11 illustrates relaxation curves for a sample with a thickness of $L = 1$ μm using model 1 ($\tilde{D} = 10^{-8}\mathrm{cm^2 s^{-1}}; \tilde{k} = 5 \times 10^{-4}\mathrm{cm\ s^{-1}}$), where the numerical simulations coincide almost perfectly with the analytical approximation (A1).

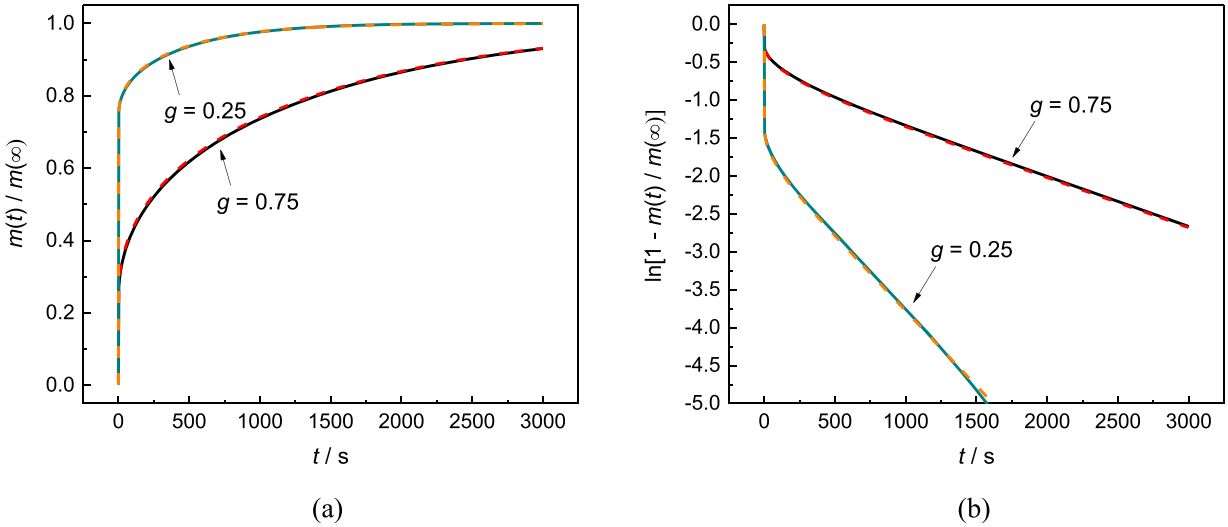

Fig. 11 **a** Relaxation curves for the total amount of exchanged oxygen for two different surface coverages g. **b** Semi-logarithmic plot of $\ln[1 - m(t)/m(\infty)]$ versus time for two different surface coverages g. Solid lines, finite element simulations (model 1); dashed lines, analytical approximation (Eq. (A1)). Sample thickness, 1 μm; cross-section of sample, 0.02 × 0.02 cm^2; thickness of surface particle, 1 μm; $\tilde{k}_{input} = 5 \times 10^{-4}$ cm s^{-1}; $\tilde{D}_{input} = 10^{-8}$ cm^2 s^{-1}

References

1. Maier J (2005) In: Conway BE, Vayenas CG, White RE (eds) Modern aspects of electrochemistry, number 38. Kluwer Academic/Plenum Publishers, New York
2. Merkle R, Maier J (2008) Angew Chem Int Ed 47(21):3874–3894
3. Lohne OF, Sogaard M, Wiik K (2013) J Electrochem Soc 160: F1282–F1292
4. Falkenstein A, Mueller DN, De Souza RA, Martin M (2015) Solid State Ionics 280:66–73
5. Preis W, Sitte W (2015) J Electroceram 34:185–206
6. Fleig J (2003) Annu Rev Mater Res 33(1):361–382
7. Preis W, Bucher E, Sitte W (2012) Fuel Cells 12(4):543–549
8. Lane JA, Kilner JA (2000) Solid State Ionics 136-137:997–1001
9. Wang S, Verma A, Yang YL, Jacobson AJ, Abeles B (2001) Solid State Ionics 140:125–133
10. Preis W, Holzinger M, Sitte W (2001) Monatsh Chem 132:499–508
11. Bouwmeester HJM, Den Otter MW, Boukamp BA (2004) J Solid State Electrochem 8:599–605
12. Preis W, Bucher E, Sitte W (2004) Solid State Ionics 175:393–397
13. Niedrig C, Wagner SF, Menesklou W, Baumann S, Ivers-Tiffee E (2015) Solid State Ionics 283:30–37
14. Li Y, Gerdes K, Diamond H, Liu X (2011) Solid State Ionics 204-205:104–110
15. Kudo H, Yashiro K, Hashimoto S, Amezawa K, Kawada T (2014) Solid State Ionics 262:696–700
16. Zhu H, Ricote S, Coors WG, Chatzichristodoulou C, Kee RJ (2014) Solid State Ionics 268:198–207
17. Preis W (2015) Comput Mater Sci 103:237–243
18. Wan TH, Saccoccio M, Chen C, Ciucci F (2015) Solid State Ionics 270:18–32
19. Blair J, Mebane DS (2015) Solid State Ionics 270:47–53
20. Preis W (2018) Solid State Ionics 316:118–124
21. Bucher E, Gspan C, Höschen T, Hofer F, Sitte W (2017) Solid State Ionics 299:26–31
22. Berger C, Bucher E, Gspan C, Menzel A, Sitte W (2018) Solid State Ionics 326:82–89
23. Jamnik J, Fleig J, Leonhardt M, Maier J (2000) J Electrochem Soc 147:3029–3035
24. Carslaw HS, Jaeger JC (1959) Conduction of heat in solids. Clarendon Press, Oxford
25. Crank J (1975) The mathematics of diffusion. Oxford University Press, Oxford
26. Preis W, Sitte W (2008) Solid State Ionics 179:765–770
27. Preis W (2009) J Phys Chem Solids 70:616–621
28. Preis W (2011) J Solid State Electrochem 15:2013–2022